Vertically Aligned WS_2 Nanosheets for Water Splitting

*Yang Yang, Huilong Fei, Gedeng Ruan, Yilun Li, and James M. Tour**

Vertically aligned WS_2 ($VAWS_2$) nanosheet films are prepared using a lithium based anodization electrolyte to fabricate WO_3 films followed by sulfurization. The $VAWS_2$ synthesized here is self-organized as a conformal structure to expose active edge sites for water splitting. These vertically aligned nanosheets are composed of exfoliated WS_2 to provide abundant active edges for catalytic reactions. Hydrogen evolution activity of the $VAWS_2$ is demonstrated to show high catalytic current, low onset overpotential and small Tafel slope. By certain measures, this $VAWS_2$ nanosheet film outperforms some of the state-of-the-art hydrogen evolution reaction (HER) catalysts, which opens up a new pathway to simply and scalably fabricate high-performance water electrolysis catalysts.

1. Introduction

Inorganic layered materials are well-recognized as 2D materials or van der Waals solids that can have unique physical properties especially when they are reduced to monolayer thicknesses.[1,2] Recently, some 2D materials, for example, the layered transition-metal dichalcogenides (LTMDs), have been identified as efficient catalysts for the HER, which is a key step toward the realization of a hydrogen-based economy through water electrolysis.[3,4] Both computational and experimental research suggests that the metallic edges of the LTMDs are catalytically active sites for HER, which enables the LTMDs to be practical alternatives to precious metals such as Pt and Pt-alloys.[5] To this end, forming LTMDs with sufficiently exposed edges through nanoengineering is required.[6] However, apart from the density and reactivity of active sites, additional factors impact the catalytic HER performance such as the electrical transport and electrical contact to the catalyst.[7] Recent studies focus on two primary paths to improve the HER performance of the LTMDs: one strategy is to control the morphology through surfaces modifications to maximize the density of active edge sites for catalysis;[8] another approach converts semiconducting phase 2H (hexagonal)-LTMDs to metallic 1T (tetragonal)-LTMDs whose bulk conduction and anisotropic electrical transport are greatly improved.[9,10]

Similar to the graphene layers in graphite, LTMDs are packed together by van der Waals interactions whereas the edges of the LTMDs are under-coordinated and thermodynamically less stable since they favor closed-shell inorganic fullerene structures when synthesized down to the nanoscale.[11] Likewise, 1T-LTMDs are metastable and cannot be found naturally on the earth.[12] The thermodynamically unfavorable nature of 1T phased LTMDs makes it challenging to find a proper synthesis technique that can afford a system for efficient HER catalysis using LTMDs. Recently 1T-LTMDs nanosheets were synthesized by chemical exfoliation using lithium-intercalation,[13–15] and this inspired our work.[16] 1T-LTMDs nanosheets, when in powder form, tend to aggregate, thereby lowering their activity.[17] Intrigued by recent success in using porous anodized films for different electrochemical applications including lithium-ion batteries, supercapacitor, and electrocatalysts,[18–21] a facile and inexpensive synthesis technique is disclosed here to form vertically aligned LTMDs nanosheet films.

2. Results and Discussion

A typical synthesis procedure of a $VAWS_2$ film is schematically shown in **Figure 1**a (for details see the Experimental Section) along with scanning electron microscope (SEM) images of the morphologies at different magnifications (Figure 1b–d): (i) W foils were anodized potentiostatically in a LiCl-containing electrolyte to form WO_3 films (Figure S1, Supporting Information). (ii) The anodized WO_3 films were reacted with sulfur vapor at 350 °C for 10 min in a chemical vapor deposition (CVD) apparatus to convert the WO_3 to the $VAWS_2$ that have abundant edges and they do not aggregate (Figure 1b–d and Figure S2, Supporting Information). More specifically, these vertically self-organized WS_2 nanosheets with flake size over 200 nm are well-dispersed and immobilized on a conductive W substrate, which can be directly used as a catalyst electrode without further treatments. Note that in conventional powder catalyst, mixing with additives, dispersing in solvent and immobilizing on a matrix are required. But these $VAWS_2$ flakes are interconnected with each other to form an open and porous framework which not only exposes the active edges but also opens up more inner surface access to the electrolyte. This synthetic approach is different than

Dr. Y. Yang,[+] H. Fei, G. Ruan, Y. Li, Prof. J. M. Tour
Department of Chemistry
Rice University
6100 Main Street, Houston, TX 77005, USA
E-mail: tour@rice.edu
Dr. Y. Yang, Prof. J. M. Tour
Smalley Institute for Nanoscale Science and Technology
Rice University
6100 Main Street, Houston, TX 77005, USA
Prof. J. M. Tour
Department of Materials Science and NanoEngineering
Rice University
6100 Main Street, Houston, TX 77005, USA
[+]Present address: NanoScience Technology Center, University of Central Florida, 12424 Research Parkway, Suite 400, Orlando, FL 32826, USA

DOI: 10.1002/adfm.201502479

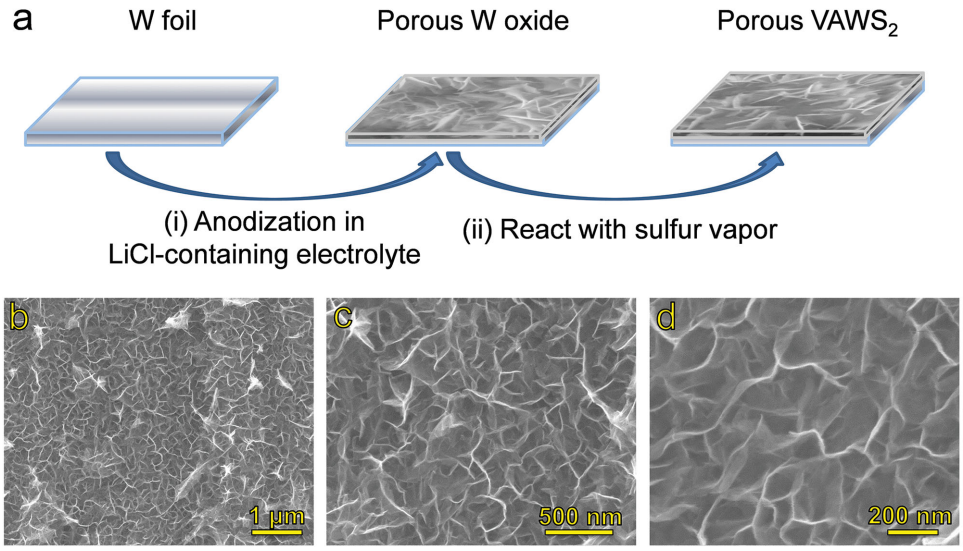

Figure 1. Schematic of the fabrication process and microscopic investigations of the $VAWS_2$ nanosheet film. a) Schematic illustration of the fabrication process. b–d) SEM images of the $VAWS_2$ film with different magnifications.

conventional anodization and other self-assembly techniques. Here, we add LiCl into the primary solution (0.15 M oxalic acid/0.1 M Na_2SO_4/0.01 M NaF aqueous solution) to do the anodization treatments and to finally obtain the $VAWS_2$ film after sulfurization. Control experiments show that without adding LiCl in the primary anodization solution, there is no sheet-like nanostructure that can be formed (see Figure S3, Supporting Information). This suggests that these vertically aligned flakes are likely to be formed by a electrochemical Li-intercalation and exfoliation of WO_3 followed by deposition on the substrate.[22]

The $VAWS_2$ was further studied by transmission electron microscopy (TEM) as shown in **Figure 2** (for more TEM images, see Figure S4, Supporting Information). Typical sheet-like flakes are clearly seen in the TEM images (Figure 2a). The layer-to-layer spacing identified from the high resolution image (HRTEM, Figure 2b,c) is in a range of 0.8 to 0.9 nm, which is much larger than conventional multilayered WS_2 and indicates the successful Li-intercalation and exfoliation of the layered WS_2.[23] In the yellow oval region in Figure 2b, two different lattice fringes are noticed, which indicates a distinguished hexagonal lattice distortion generated in the $VAWS_2$.[8] This is ascribed to the inner strain induced by Li-doping/intercalation and the phase transition from 2H to 1T phase.[24] Clear lattice fringes from the WS_2 basal plane are presented in Figure 2d and from the diffraction pattern (inset of Figure 2b) converted from the marked square area in Figure 2b.

The complete chemical conversion from WO_3 to WS_2 can be identified from the strong diffraction peaks in the XRD patterns of **Figure 3**a that are all indexed to the WS_2 according to JCPDS card no. 08–0237. A significant difference is demonstrated from the (002) peak (Figure 3b), where a new diffraction peak located at ≈13° is observed along with a (002) diffraction shifted to lower angle. These are convincing indications of the lattice expansion effect in the Li-intercalated compounds.[25] An easily overlooked feature is the appearance of the (001) peak (Figure 3c) after Li-intercalation/exfoliation, which is further evidence for the exfoliation of WS_2.[26]

Raman spectroscopy is a superior technique to investigate the layered structure of WS_2 through analyzing the vibration modes of A_{1g} at 420 cm^{-1} and E^1_{2g} at 354 cm^{-1}, which represent the out-of-plane W–S phonon mode and the in-plane W–S phonon mode, respectively.[27] The intensity ratio of E^1_{2g}/A_{1g} is a fingerprint signal for characteristics of layered WS_2, such as grain size, layer number and exposed edge sites.[28] Hence, the apparent increase in the relative intensity of E^1_{2g}/A_{1g} (Figure 3d) from ≈0.75 (non-nanostructured WS_2) to 1.21 ($VAWS_2$) indicates

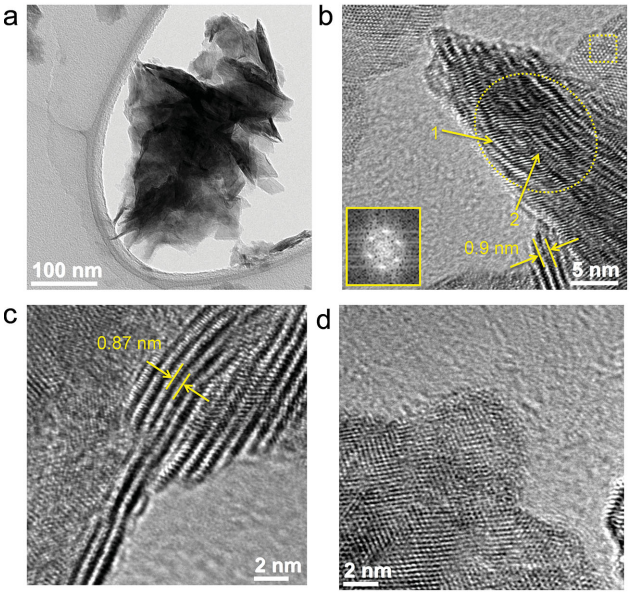

Figure 2. TEM analysis of the $VAWS_2$ film. a) A TEM image of the $VAWS_2$. b) High resolution TEM (HRTEM) image of the $VAWS_2$. The inset is the corresponding diffraction pattern converted from the marked yellow square region. The marked oval region shows the distorted lattice fringes. Lattice-1 and lattice-2 marked show different lattice fringes, which indicates a lattice distortion. c) HRTEM image of the $VAWS_2$ interlayer distance. d) HRTEM image of the $VAWS_2$ basal plane.

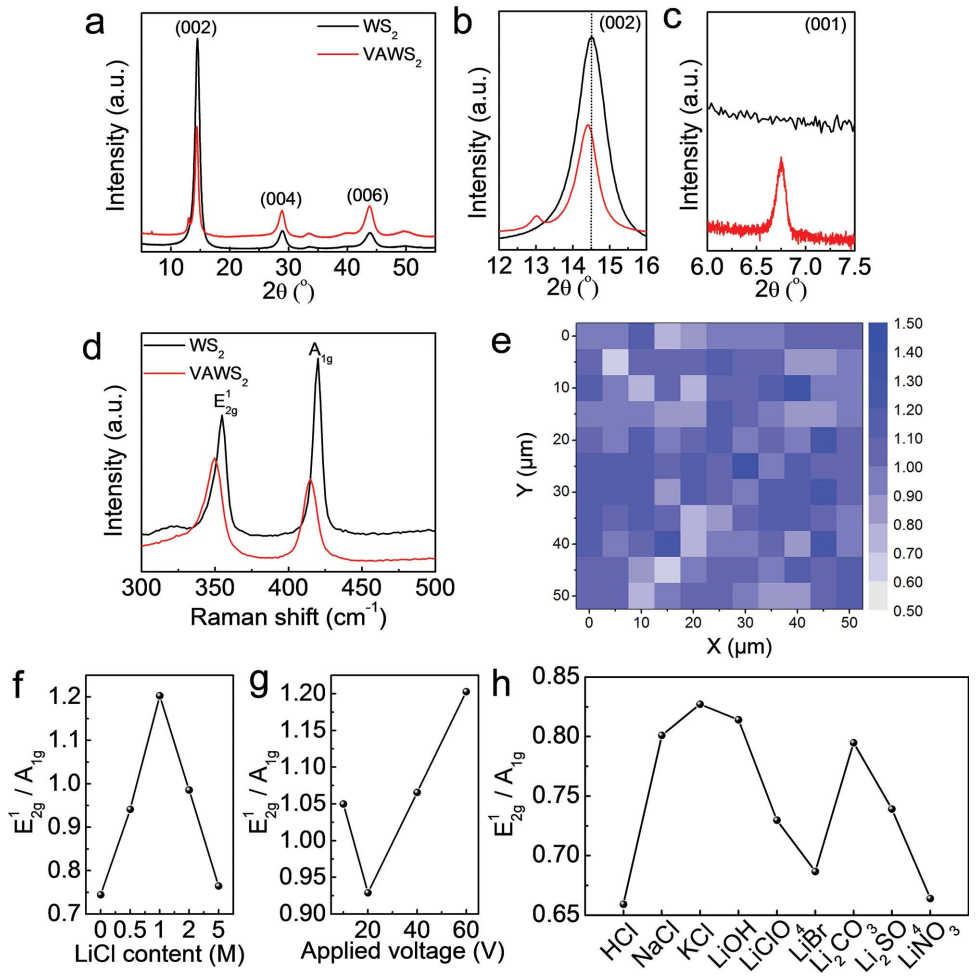

Figure 3. Structural investigations of the $VAWS_2$ film. a) XRD patterns of the WS_2 films. b,c) XRD patterns of the WS_2 (002) and (001) planes, respectively. d) Raman spectra of the WS_2 films. e) Raman map of the $VAWS_2$ film in an area of 55×55 μm^2 with an interval of 5 μm. This plot was generated using the intensity ratio of the E^1_{2g}/A_{1g} peaks obtained from the Raman spectra. f–h) Intensity ratio of E^1_{2g}/A_{1g} varied with LiCl content in the anodization solution, applied voltage and different additives, respectively.

the reduced layer number by the exfoliation of WS_2, while increasing the exposed active edges. Compared to non-nanostructured WS_2, the slightly blue-shifted E^1_{2g} and A_{1g} phonon modes of the $VAWS_2$ are from the inner strain generated in the nanostructured WS_2.[29] To further characterize the homogeneity of the monolayer of WS_2, Raman mapping analysis was performed over an area of 55×55 μm^2 at an interval of 5 μm. From the isotope-labeled image plotted by the intensity ratio of E^1_{2g}/A_{1g}, most of the investigated area has an intensity ratio >1, which indicates the $VAWS_2$ is composed of exfoliated WS_2 nanosheets (Figure 3e).

To understand how LiCl and other alkali metal-salts facilitate the formation of the $VAWS_2$ nanosheets, a series of comparative experiments were carried out using the intensity ratios of E^1_{2g}/A_{1g} in the Raman spectra. We added different amounts of LiCl from 0 to 5 M in the primary anodization solution to do the anodization treatment on W foil at 60 V for 1 min (Figure 3f). The number of S–W–S layers decreases and the exposed edges increase with increased amount of LiCl and it finally converged in 1 M LiCl-containing solution. However, because of the heating effect induced by high cation concentration in the anodization solution, adding more LiCl in the anodization solution adds no further improvement to the exfoliation of WS_2 and actually shows a detrimental effects where the layering increase (Figure 3f). A commonly encountered problem in conventional anodization processes is that heating causes damage to the self-organized nanostructures, and that happened here when we applied voltage to the anodization solution with excessive LiCl being present (see Figure S5, Supporting Information).[30]

We investigated the impact of the applied voltage used in the anodization on the number of S–W–S layers and exposed edge sites (Figure 3g and for more Raman analyses see Figure S6, Supporting Information), where we measured a quasilinear increase in the intensity ratio of E^1_{2g}/A_{1g}. The facilitated Li-intercalation and exfoliation by increasing the applied voltage shows an apparent improvement on the exfoliation and exposing in edges sites in $VAWS_2$.[31] However, any attempt to further increase the applied voltage over 60 V causes extreme heating, which destroys the $VAWS_2$ film.

To optimize the Li-salt usage in the $VAWS_2$ film forming process, different alkali metal-salts and HCl with molarities of 1 M were added to the anodization solution (Figure 3h). A set of control experiments were designed to examine whether the

different alkali metal ions and H^+ are of any help in the exfoliation of WS_2. From the intensity ratio of E^1_{2g}/A_{1g}, HCl has no positive impact on reducing the number of S–W–S layers because the anodized oxide layer is easier to dissolve in a more acidic solution instead of forming a self-organized nanostructure.[32] And other alkali metal chlorides (NaCl and KCl) can only form a insufficiently exfoliated WS_2, compared to when literature is used.[33] Another set of control experiments were performed with different Li-salts (in the concentration of 1 M), and apart from LiCl, other Li-salts (for a list of Li-salts, see Figure 3h) only form a poorly exfoliated or even bulk WS_2. This suggests that chloride-assisted Li-intercalation and exfoliation are favored during electrochemical anodization treatment, likely due to the smaller ionic radius of both Li^+ and Cl^- compared to the other soluble Li-salts examined in this work. However, due to the low solubility of LiF in water at room temperature, LiF did not work properly for Li-intercalation/exfoliation in our case.

X-ray photoelectron spectroscopy (XPS) shows clear signals for W 4f and S 2p peaks in the WS_2 (for detailed XPS discussion, see the Supporting Information and Figure S7). The observed Li 1s peak has a binding energy closer to that in the Li-intercalated layered materials, which is from the Li-dopant formed in the Li-intercalation/exfoliation process.

Exploring the unique vertically aligned and interconnected edges in the $VAWS_2$ porous films, their HER activities were studied. Conveniently, the $VAWS_2$ film (loading mass ≈150 μg cm^{-2}) grown on W foil can be directly used as an electrode for HER testing without adding any additives such as conductive carbon and polymer binders. The excellent HER activity of the $VAWS_2$ film was first confirmed by linear sweep voltammetry (LSV) curves (**Figure 4**a) and their corresponding

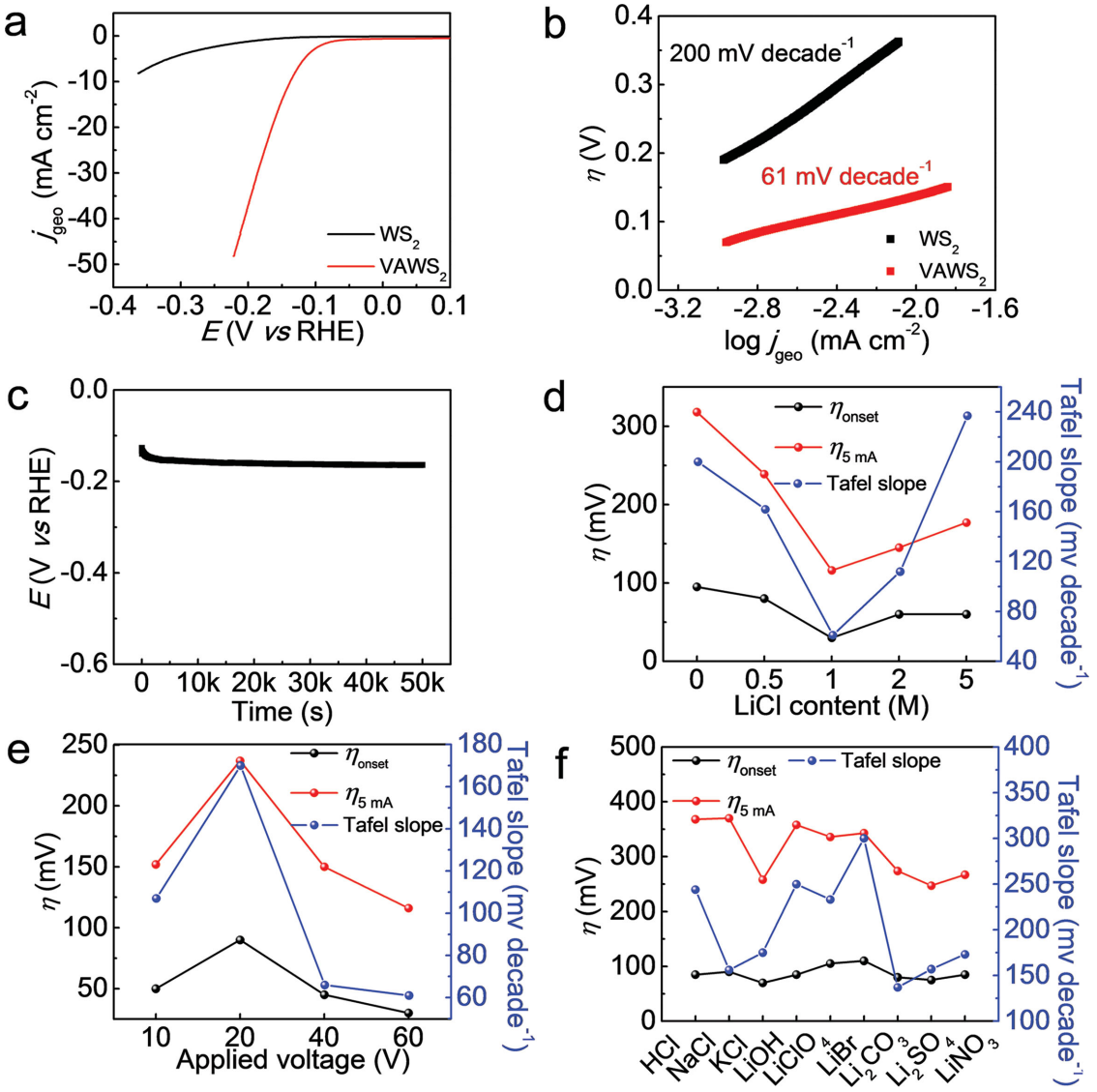

Figure 4. Electrochemical HER activity of the $VAWS_2$ film. a,b) Linear sweep voltammetry (LSV) curves measured at 5 mV s^{-1} in 0.5 M H_2SO_4 aqueous solution and corresponding Tafel slopes. c) 50 000 s durability test in 0.5 M H_2SO_4 aqueous solution. d–f) HER activities of the $VAWS_2$ films varied with LiCl content in the anodization solution, applied voltage and different additives, respectively.

Tafel plots (Figure 4b) tested in acidic solution (0.5 M H_2SO_4). The HER onset overpotential (η) of the $VAWS_2$ film is ≈30 mV, which is much better than the non-nanostructured WS_2 and superior to most of the reported WS_2 systems (for a detailed comparison, see Table S1, Supporting Information). The maximum iR-corrected kinetic current density (j_{geo}) normalized to the geometric area can reach 10 and 48 mA cm^{-2} at $\eta \approx 136$ and 221 mV, respectively, which is also better than the non-nanostructured WS_2 film and other forms of WS_2 (Table S1, Supporting Information). The corresponding Tafel slope of the $VAWS_2$ film is ≈61 mV $decade^{-1}$ (Figure 4b). This indicates that the Volmer reaction is active, a process that converts protons into absorbed hydrogen atoms, and this is the rate-determining step in the HER mechanism of the $VAWS_2$ films.[34] However, a Tafel slope ≈200 mV $decade^{-1}$ is observed in the non-nanostructured WS_2 film, which indicates that an unfacilitated charge transfer process dominates HER kinetics in the compact WS_2 film.[35] Moreover, durability testing was performed on the $VAWS_2$ films galvanostatically at 10 mA cm^{-2} for 50k s (Figure 4c). The HER catalytic activity for the $VAWS_2$ film is stable over long-term testing and a slight decay observed in the initial few minutes is from the physically adsorbed H_2 bubbles on the electrode surface. The HER activity of the WS_2 films in the control experiments (varied LiCl concentration, different applied voltages and different additives) was also measured (Figure 4d–f and Figures S8–S10, Supporting Information). Through comparing the η_{onset}, $\eta_{5\ mA}$ (overpotential at a current density of 5 mA cm^{-2}), and Tafel slopes, it is not surprising to see that the HER activity is quasi-proportional to the exfoliation extent of WS_2. Recently, anion-doping with P and Cl was studied as an effective way to modify the electronic structure of LTMDs and to improve their catalytic performances.[36] Here, through investigating the HER performance of the WS_2 films obtained from different alkali metal chlorides and HCl, we conclude that Cl^- does not play a decisive role in enhancing the HER activity of the $VAWS_2$ film because we did not find Cl in the $VAWS_2$ film through XPS analysis. Therefore, compared to the non-nanostructured WS_2 film, the $VAWS_2$ film delivers superior HER activity which likely benefits from the fully exposed edges and more open access to the electrolyte by forming interconnected porous structures in the $VAWS_2$ film.[37] Furthermore, the stabilized 1T phased WS_2 in the strained $VAWS_2$ films also contribute to their superior HER performance.

3. Conclusions

In summary, vertically aligned WS_2 nanosheet films were fabricated through an in situ LiCl-assisted exfoliation/deposition of WO_3 via an anodization followed by low temperature sulfurization. The sufficiently exposed WS_2 edges and porous structure make this WS_2 film an excellent HER material with long-term durability. The inner strain induced by partially Li-doping and transition to 1T phase of WS_2 also makes the film active for catalytic reactions. The superior HER activity is a clear indication that the catalytic performance of the LTMDs could be greatly enhanced through nanoengineering. This proposed fabrication technique and the basic concept of using nanoengineering to tailor the catalytic activity of LTMDs opens a new direction in designing efficient catalysts.

4. Experimental Section

Fabrication: To prepare $VAWS_2$ films, W foils (0.785 cm^2 in area, 0.05 mm in thickness, 99.9%, Sigma-Aldrich, USA) were used as substrates and before use were cleaned and degreased by sonication (Cole Parmer, model 08849–00) sequentially in isopropanol and acetone each for 30 min, respectively. Electrochemical anodization was carried out at room temperature in a mixed solution of 0.15 M oxalic acid/0.1 M Na_2SO_4/0.01 M NaF in DI-water with additional 1 M lithium-salts (LiCl, LiOH, $LiCLO_4$, LiBr, Li_2CO_3, Li_2SO_4, and $LiNO_3$) as additives to grow WO_3 films. Anodization was conducted at 60 V in a two electrode set-up with platinum foil as the counter electrode. To form $VAWS_2$, the anodized WO_3 was placed at the center of a 2.54 cm quartz tube furnace. Sulfur powder (Sigma-Aldrich) was placed at the upstream side 2 cm away from the tube furnace center. The tube was evacuated to a base pressure of ≈50 mTorr for at least 10 min and flushed with Ar to remove the residual air. Then, the furnace center was set to 350 °C within 10 min, and the sulfur powder was kept in the temperature zone ≈250 °C. The reaction was allowed to proceed for 20 min with Ar (100 sccm) as a carrier gas, followed by permitting the tube cool to room temperature after the reaction.

Characterization: Microscopic investigations were performed using a JEOL 6500F SEM and a JEOL 2010 HRTEM. To prepare the TEM sample, the $VAWS_2$ film was stripped from the metal substrate by scratching with blade and bath sonicated (20 W Cole–Palmer Ultrasonicator Model 08849–00) in 5 mL of ethanol for 30 min. After this the entire 5 mL solution (well dispersed $VAWS_2$ in ethanol) was transferred to a TEM grid and dried under ambient conditions for 12 h before characterization. The crystal structure of the $VAWS_2$ film was analyzed by XRD using a Rigaku D/Max Ultima II (Rigaku Corporation, Japan) diffractometer configured with a CuKα radiation source. Raman spectra were recorded with a Renishaw Raman RE01 scope (Renishaw Inc., USA) using a 514 nm excitation argon laser. Raman mapping was obtained in an area of 55 × 55 μm^2 with an interval of 5 μm. The Figure 3e was plotted using the intensity ratio of E^1_{2g}/A_{1g} peaks. Chemical compositions of the thin films were checked by XPS (PHI Quantera XPS, Physical Electronics, USA). An Al anode at 25 W was used as an X-ray source with a pass energy of 26.00 eV, 45° take off angle, and a 100 μm beam size. A pass energy of 140 eV was used for the survey and 26 eV for the atomic concentration.

Electrochemical Measurement: The $VAWS_2$ films grown on W metals were directly used as working electrodes for the electrochemical measurements. The electrocatalytic HER performance was tested in a H_2-saturated 0.5 M H_2SO_4 electrolyte with a platinum foil and K_2SO_4-saturated $Hg/HgSO_4$ electrode (CHI) as the counter and reference electrodes, respectively, within a three electrode set-up. The reference electrode is calibrated in a H_2-saturated electrolyte with respect to a reverse hydrogen electrode (RHE). LSV was performed at a scan rate of 5 mV s^{-1}. All the electrochemical characterizations were carried out with an electrochemical analyzer (CHI 608D, CH Instruments, USA).

Supporting Information

Supporting Information is available from the Wiley Online Library or from the author.

Acknowledgements

The authors thank the AFOSR MURI program (FA9550–14–1–0111) for their financial support.

Received: June 17, 2015
Revised: August 3, 2015
Published online: September 11, 2015

[1] K. S. Novoselov, D. Jiang, F. Schedin, T. J. Booth, V. V. Khotkevich, S. V. Morozov, A. K. Geim, *Proc. Natl. Acad. Sci. USA* **2005**, *102*, 10451.
[2] W. J. Lee, U. N. Maiti, J. M. Lee, J. Lim, T. H. Han, S. O. Kim, *Chem. Commun.* **2014**, *50*, 6818.
[3] D. J. Li, U. N. Maiti, J. Lim, D. S. Choi, W. J. Lee, Y. Oh, G. Y. Lee, S. O. Kim, *Nano Lett.* **2014**, *14*, 1228.
[4] D. Voiry, M. Salehi, R. Silva, T. Fujita, M. Chen, T. Asefa, V. B. Shenoy, G. Eda, M. Chhowalla, *Nano Lett.* **2013**, *13*, 6222.
[5] Y. Li, H. Wang, L. Xie, Y. Liang, G. Hong, H. Dai, *J. Am. Chem. Soc.* **2011**, *133*, 7296.
[6] Z. Liu, M. Amani, S. Najmaei, Q. Xu, X. Zou, W. Zhou, T. Yu, C. Qiu, A. G. Birdwell, F. J. Crowne, R. Vajtai, B. I. Yakobson, Z. Xia, M. Dubey, P. M. Ajayan, J. Lou, *Nat. Commun.* **2014**, *5*, 5246.
[7] M. A. Lukowski, A. S. Daniel, F. Meng, A. Forticaux, L. Li, S. Jin, *J. Am. Chem. Soc.* **2013**, *135*, 10274.
[8] C. Tsai, K. Chan, F. Abild-Pedersen, J. K. Nørskov, *Phys. Chem. Chem. Phys.* **2014**, *16*, 13156.
[9] F. Wypych, R. Schöllhorn, *Chem. Commun.* **1992**, *19*, 1386.
[10] Q. Liu, X. Li, Z. Xiao, Y. Zhou, H. Chen, A. Khalil, T. Xiang, J. Xu, W. Chu, X. Wu, J. Yang, C. Wang, Y. Xiong, C. Jin, P. M. Ajayan, L. Song, *Adv. Mater.* **2015**, DOI: 10.1002/adma.201502134.
[11] Y. Feldman, E. Wasserman, D. J. Srolovitz, R. Tenne, *Science* **1995**, *267*, 222.
[12] A. N. Enyashin, L. Yadgarov, L. Houben, I. Popov, M. Weidenbach, R. Tenne, M. Bar-Sadan, G. Seifert, *J. Phys. Chem. C* **2011**, *115*, 24586.
[13] G. Eda, H. Yamaguchi, D. Voiry, T. Fujita, M. Chen, M. Chhowalla, *Nano Lett.* **2011**, *11*, 5111.
[14] D. Voiry, H. Yamaguchi, J. Li, R. Silva, D. C. B. Alves, T. Fujita, M. Chen, T. Asefa, V. B. Shenoy, G. Eda, M. Chhowalla, *Nat. Mater.* **2013**, *12*, 850.
[15] J. Xiao, D. Choi, L. Cosimbescu, P. Koech, J. Liu, J. P. Lemmon, *Chem. Mater.* **2010**, *22*, 4522.
[16] V. Nicolosi, M. Chhowalla, M. G. Kanatzidis, M. S. Strano, J. N. Coleman, *Science* **2013**, *340*, 6139.
[17] C. H. Bartholomew, *Appl. Catal. A: General* **2001**, *212*, 17.
[18] Y. Yang, G. Ruan, C. Xiang, G. Wang, J. M. Tour, *J. Am. Chem. Soc.* **2014**, *136*, 6187.
[19] Y. Yang, Z. Peng, G. Wang, G. Ruan, X. Fan, L. Li, H. Fei, R. H. Hauge, J. M. Tour, *ACS Nano* **2014**, *8*, 7279.
[20] Y. Yang, H. Fei, G. Ruan, C. Xiang, J. M. Tour, *ACS Nano* **2014**, *8*, 9518.
[21] Y. Yang, H. Fei, G. Ruan, C. Xiang, J. M. Tour, *Adv. Mater.* **2014**, *26*, 8163.
[22] M. A. Lukowski, A. S. Daniel, C. R. English, F. Meng, A. Forticaux, R. J. Hamers, S. Jin, *Energy Environ. Sci.* **2014**, *7*, 2608.
[23] H. A. Hamedani, N. K. Allam, H. Garmestani, M. A. El-Sayed, *J. Phys. Chem. C* **2011**, *115*, 13480.
[24] M. Krause, A. Mücklich, A. Zak, G. Seifert, S. Gemming, *Physica Status Solidi B* **2011**, *248*, 2716.
[25] Z. Chen, D. Cummins, B. N. Reinecke, E. Clark, M. K. Sunkara, T. F. Jaramillo, *Nano Lett.* **2011**, *11*, 4168.
[26] J. Zheng, H. Zhang, S. Dong, Y. Liu, C. T. Nai, H. S. Shin, H. Y. Jeong, B. Liu, K. P. Loh, *Nat. Commun.* **2014**, *5*, 2995.
[27] S. Jeong, D. Yoo, M. Ahn, P. Miró, T. Heine, J. Cheon, *Nat. Commun.* **2015**, *6*, 5763.
[28] H. S. S. R. Matte, A. Gomathi, A. K. Manna, D. J. Late, R. Datta, S. K. Pati, C. N. R. Rao, *Angew. Chem.* **2010**, *122*, 4153.
[29] A. Berkdemir, H. R. Gutiérrez, A. R. Botello-Méndez, N. Perea-López, A. L. Elías, C. -I. Chia, B. Wang, V. H. Crespi, F. López-Urías, J.-C. Charlier, H. Terrones, M. Terrones, *Sci. Rep.* **2012**, *3*, 1755.
[30] Y. Yang, S. P. Albu, D. Kim, P. Schmuki, *Angew. Chem.* **2011**, *123*, 9237.
[31] J. N. Reimers, J. R. Dahn, *J. Electrochem. Soc.* **1992**, *139*, 2091.
[32] J. Bai, B. Zhou, L. Li, Y. Liu, Q. Zheng, J. Shao, X. Zhu, W. Cai, J. Liao, L. Zou, *J. Mater. Sci.* **2008**, *43*, 1880.
[33] M. Qureshi, A. Ahmad, *Solvent Extr. Ion Exch.* **1986**, *4*, 823.
[34] N. Pentland, J. O. M. Bockris, E. Sheldon, *J. Electrochem. Soc.* **1957**, *104*, 182.
[35] N. Danilovic, R. Subbaraman, D. Strmcnik, K. -C. Chang, A. P. Paulikas, V. R. Stamenkovic, N. M. Markovic, *Angew. Chem.* **2012**, *124*, 12663.
[36] J. Kibsgaard, T. F. Jaramillo, *Angew. Chem. Int. Ed.* **2014**, *53*, 14433.
[37] C. Jo, Y. Seo, K. Cho, J. Kim, H. S. Shin, M. Lee, J. C. Kim, S. O. Kim, J. Y. Lee, H. Ihee, R. Ryoo, *Angew. Chem. Int. Ed.* **2014**, *53*, 5117.